Available online at www.sciencedirect.com
ScienceDirect
Chinese Journal of Aeronautics 20(2007) 452-463
Chinese Journal of Aeronautics
www.elsevier.com/locate/cja

Earth-moon Trajectory Optimization Using Solar Electric Propulsion

Gao Yang*

Academy of Opto-Electronics, Chinese Academy of Sciences, Beijing 100080, China

Received 5 April 2007; accepted 17 August 2007

Abstract

The optimization of the Earth-moon trajectory using solar electric propulsion is presented. A feasible method is proposed to optimize the transfer trajectory starting from a low Earth circular orbit (500 km altitude) to a low lunar circular orbit (200 km altitude). Due to the use of low-thrust solar electric propulsion, the entire transfer trajectory consists of hundreds or even thousands of orbital revolutions around the Earth and the moon. The Earth-orbit ascending (from low Earth orbit to high Earth orbit) and lunar descending (from high lunar orbit to low lunar orbit) trajectories in the presence of J_2 perturbations and shadowing effect are computed by an analytic orbital averaging technique. A direct/indirect method is used to optimize the control steering for the trans-lunar trajectory segment, a segment from a high Earth orbit to a high lunar orbit, with a fixed thrust-coast-thrust engine sequence. For the trans-lunar trajectory segment, the equations of motion are expressed in the inertial coordinates about the Earth and the moon using a set of nonsingular equinoctial elements inclusive of the gravitational forces of the sun, the Earth, and the moon. By way of the analytic orbital averaging technique and the direct/indirect method, the Earth-moon transfer problem is converted to a parameter optimization problem, and the entire transfer trajectory is formulated and optimized in the form of a single nonlinear optimization problem with a small number of variables and constraints. Finally, an example of an Earth-moon transfer trajectory using solar electric propulsion is demonstrated.

Keywords: trajectory optimization; solar electric propulsion; analytic orbital averaging technique; direct/indirect method

1 Introduction

Since the Deep Space 1 spacecraft demonstrated the first use of solar electric propulsion (SEP) for an interplanetary mission[1], the application of low-thrust propulsion for future space missions has been a popular research subject. More recently, the ESA Smart-1 spacecraft[2] launched in 2003 successfully performed the first lunar mission using solar electric propulsion. It is well known that the spacecraft propelled by low-thrust SEP engines is capable of delivering a greater payload fraction compared to the spacecraft using conventional chemical propulsion. However, the low-thrust continuous control profiles can not be approximated by the impulsive velocity differences. How to optimize low-thrust transfer trajectories becomes a new challenge to the mission designers who want to use SEP as the primary spacecraft propulsion.

In the past two decades, lots of researches on low-thrust Earth-moon trajectories were conducted. For instance, Golan and Breakwell[3] investigated minimum-fuel lunar trajectories with the fixed transfer time by patching Earth- and moon-centered spirals at an intermediate point. Huelman[4] introduced a power-limited optimal guidance law for Earth-moon transfers in a planar restricted three-

*Corresponding author. Tel.: +86-10-62582810.
E-mail address: gaoy@aoe.ac.cn
Foundation item: National Natural Science Foundation of China (10603005)

body dynamics. Piersion and Kluever[5] solved optimal Earth-moon trajectories using a three-stage approach. Later, they obtained a series of Earth-moon trajectories[6-8] in the classical restricted three-body dynamics. Herman and Conway[9] employed a parallel Runge-Kutta method to solve optimal Earth-moon transfers, which start from a circular orbit with 6.3 Earth radii and end at a two-lunar-radii orbit. The initial thrust acceleration of $10^{-4}g_0$ (g_0 is the Earth sea-level gravitational acceleration) yields a 32-day flight journey. Recently, Betts[10] obtained an optimal trajectory from a geostationary transfer orbit (GTO) to a high elliptic lunar orbit with the perilune radius of 2 378 km and the apolune radius of 11 738 km using the direct transcription method or collocation method, which creates a large-scale nonlinear optimization problem including 211 031 variables and 146 285 constraints. A less accurate approximate solution to this problem was obtained with the computational time of 4.2×10^4 s (11.67 h) and the longer time is needed to obtain a more accurate solution.

However, complete transfers from low Earth orbits (LEO) to low lunar orbits (LLO) using solar electric propulsion with or without consideration of significant shadowing effect still have not been solved in above-mentioned papers. In Refs.[7] and [8], Kluever and Piersion used the Edelbaum's method to approximate the spirals from LEO to a high Earth orbit (HEO), and from a high lunar orbit (HLO) to LLO. Nevertheless, the Edelbaum's method does not consider J_2 perturbations and shadowing condition that significantly affects trajectory evolution in relatively low-altitude orbits around the Earth and the moon. If Betts' direct transcription and the parallel Runge-Kutta method[9] are utilized to solve a long-duration transfer trajectory from LEO to LLO, the dimension of the nonlinear optimization problem would be much larger. In addition, it is difficult to consider the shadowing effect in the existing direct methods.

This paper demonstrates a feasible method to compute the low-thrust Earth-moon trajectory from a low earth circular orbit (500 km altitude) to a low lunar circular orbit (200 km altitude). The transfer from HEO to HLO is computed by a direct/indirect method utilized by Kluever and Piersion[5-8], but the equinoctial elements in a four-body (the Earth, the moon, the sun, and the spacecraft) dynamics including J_2 perturbations are employed. Furthermore, the low-thrust spirals from LEO to HEO and from HLO to LLO are computed by an analytic orbital averaging technique (AOAT), in which the third-body perturbations are ignored but the significant J_2 perturbations and shadowing effect are taken into account. The ephemeris of the Earth, the moon, and the sun are obtained using JPL planetary and lunar ephemerides[11]. The moon's orbit around the Earth is not a planar circular orbit; the moon's inclination varies between 18° and 28° every 15 years. The entire trajectory is assumed to be a burn-coast-burn sequence, which is a good tradeoff between fuel consumption and transfer time. The optimal control problem for the Earth-moon transfer trajectory is converted to a parameter optimization problem that is in turn solved by nonlinear programming—sequential quadratic programming (SQP). The entire transfer trajectory is optimized by a single nonlinear SQP problem including only a few variables and constraints.

2 Equations of Motion

2.1 Definitions of ECI and MCI coordinates

The ECI coordinate (Earth-centered inertial coordinate $O_e x_e y_e z_e$, see Fig.1) refers to the J2000 Earth equatorial frame that is defined by the mean orientation of the Earth's equator and ecliptic orbit at the beginning of the year 2000. The $O_e x_e y_e$ plane is parallel to the mean Earth's equator. The line formed by intersection of the ecliptic orbit plane and the Earth's equatorial plane, defines the axis x_e. The line, on the first day of autumn (starting from the sun to the center of the Earth) defines the positive direction of the axis x_e, which is called the vernal equinox. The axis z_e is perpendicular to the $O_e x_e y_e$ plane and points to the north. The axis y_e completes the Cartesian coordinate using the right-handed

principle. The MCI coordinate, i.e. moon-centered inertial coordinate $O_m x_m y_m z_m$ (Fig.1) is parallel to $O_e x_e y_e z_e$ with different origins. In this paper, the equations of motion in both ECI and MCI coordinates are expressed by a set of equinoctial elements[12-14], which avoid singularities when the orbit's inclination and eccentricity equal to zero.

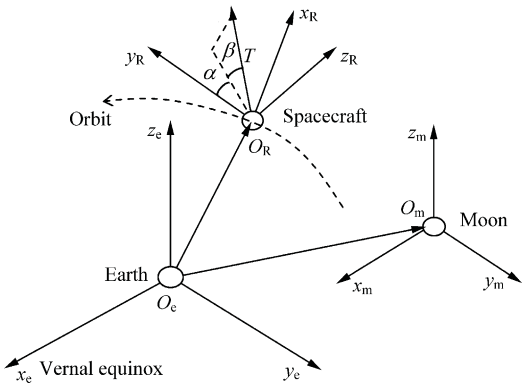

Fig.1 Illustrations of ECI, MCI coordinates and thrust steering angles in the local rotating coordinate $O_R x_R y_R z_R$, where the axis x_R is from the Earth to the spacecraft, the axis z_R is perpendicular to the orbital plane, and the axis y_R completes the Cartesian coordinate $O_R x_R y_R z_R$ following the right-handed principle, which is in the orbital plane and points to the velocity direction.

2.2 Equations of motion in the ECI coordinate

The equations of motion in the ECI coordinate for the Earth-departure trajectory are

$$\dot{\boldsymbol{x}} = \boldsymbol{M}\left(\frac{T}{m}\boldsymbol{\alpha}_T + \boldsymbol{\alpha}_{J_2-\text{Earth}} + \boldsymbol{\alpha}_{\text{moon}} + \boldsymbol{\alpha}_{\text{sun}_1}\right) + \boldsymbol{D} \quad (1)$$

$$\dot{m} = -T/(g_0 I_{\text{sp}}) \quad \text{where} \quad T = 2\eta P/(g_0 I_{\text{sp}}) \quad (2)$$

where $\boldsymbol{x} = [p\ f\ g\ h\ k\ L]^T$ is the vector of equinoctial elements in the ECI coordinate, and $\boldsymbol{\alpha}_{J_2-\text{Earth}}$, $\boldsymbol{\alpha}_{\text{moon}}$, and $\boldsymbol{\alpha}_{\text{sun}_1}$ are Earth J_2 oblateness acceleration, moon's perturbation, and sun's perturbation respectively in the ECI coordinate. The elements in the matrices $\boldsymbol{M}$ and $\boldsymbol{D}$ are given in Appendix A. Eq.(2) is the mass flow rate, where T is thrust amplitude, and P, I_{sp}, and η are power, specific impulse and efficiency of the SEP system, respectively. The thrusting direction unit vector can be expressed in terms of local pitch and yaw steering angles

$$\boldsymbol{\alpha}_T = \begin{bmatrix}\sin\alpha\cos\beta & \cos\alpha\cos\beta & \sin\beta\end{bmatrix}^T \quad (3)$$

where the pitch angle (α) is measured from the local horizon (the axis $\boldsymbol{y}_R$) to the projection of the thrust vector onto the orbit plane, and the yaw angle (β) is measured from the orbit plane to the thrust vector (see Fig.1).

The Earth gravitational parameter and Earth radius (μ_e and R_e) define the non-dimensional units—distance, velocity, time, and acceleration—in the ECI coordinate as follows

$$\tilde{d}_e = R_e,\ \tilde{v}_e = \sqrt{\frac{\mu_e}{R_e}},\ \tilde{t}_e = \frac{R_e}{\tilde{v}_e},\ \tilde{a}_e = R_e/\tilde{t}_e^2 \quad (4)$$

The Earth J_2 perturbations can be expressed in the rotating coordinate $O_R x_R y_R z_R$

$$\boldsymbol{\alpha}_{J_2-\text{Earth}} = \begin{bmatrix} -\dfrac{3\mu_e J_{2e} R_e^2}{2r^4}\left[1 - \dfrac{12(h\sin L - k\cos L)^2}{(1+h^2+k^2)^2}\right] \\ -\dfrac{12\mu_e J_{2e} R_e^2}{r^4}\dfrac{(h\sin L - k\cos L)(h\cos L + k\sin L)}{(1+h^2+k^2)^2} \\ -\dfrac{6\mu_e J_{2e} R_e^2}{r^4}\dfrac{(1-h^2-k^2)(h\sin L - k\cos L)}{(1+h^2+k^2)^2} \end{bmatrix} \quad (5)$$

where r is the distance from the Earth center to the spacecraft. The gravitational accelerations of the sun and the moon expressed in the ECI coordinate can be written as

$$\tilde{\boldsymbol{\alpha}}_{\text{sun}_1} = -\mu_{\text{sun}}\left(\frac{\boldsymbol{r}_{\text{sun-sc}}}{\|\boldsymbol{r}_{\text{sun-sc}}\|^3} + \frac{\boldsymbol{r}_{\text{e-sun}}}{\|\boldsymbol{r}_{\text{e-sun}}\|^3}\right) \quad (6)$$

$$\tilde{\boldsymbol{\alpha}}_{\text{moon}} = -\mu_{\text{m}}\left(\frac{\boldsymbol{r}_{\text{m-sc}}}{\|\boldsymbol{r}_{\text{m-sc}}\|^3} + \frac{\boldsymbol{r}_{\text{e-m}}}{\|\boldsymbol{r}_{\text{e-m}}\|^3}\right) \quad (7)$$

where $\boldsymbol{r}_{\text{sun-sc}}$ is the position vector from the sun to the spacecraft, $\boldsymbol{r}_{\text{e-sun}}$ from the Earth to the sun, $\boldsymbol{r}_{\text{m-sc}}$ from the moon to the spacecraft, and $\boldsymbol{r}_{\text{e-m}}$ from the Earth to the moon. The gravitational parameters of the sun and the moon are denoted by μ_{sun} and μ_{m}, respectively. The vector $\tilde{\boldsymbol{\alpha}}_{\text{sun}_1}$ and $\tilde{\boldsymbol{\alpha}}_{\text{moon}}$ in the ECI coordinate should be transformed to $\boldsymbol{\alpha}_{\text{sun}_1}$ and $\boldsymbol{\alpha}_{\text{moon}}$ in the local rotating coordinate.

2.3 Equations of motion in the MCI coordinate

Likewise, the equations of motion in the MCI coordinate for the moon-capture trajectory are

$$\dot{\boldsymbol{x}}_2 = \boldsymbol{M}_2\left(\frac{T}{m}\boldsymbol{\alpha}_{\mathrm{T}} + \boldsymbol{\alpha}_{J_2-\mathrm{moon}} + \boldsymbol{\alpha}_{\mathrm{Earth}} + \boldsymbol{\alpha}_{\mathrm{sun}_2}\right) + \boldsymbol{D}_2 \quad (8)$$

where $\boldsymbol{x}_2 = [p_2\ f_2\ g_2\ h_2\ k_2\ L_2]^{\mathrm{T}}$ is the vector of equinoctial elements in the MCI coordinate, and $\boldsymbol{\alpha}_{J_2-\mathrm{moon}}$, $\boldsymbol{\alpha}_{\mathrm{Earth}}$, and $\boldsymbol{\alpha}_{\mathrm{sun}_2}$ are moon J_2 oblateness acceleration, Earth's perturbation, and sun's perturbation respectively in the MCI coordinate. The elements in the matrices $\boldsymbol{M}_2$ and $\boldsymbol{D}_2$ are in the expressions as in the matrices $\boldsymbol{M}$ and $\boldsymbol{D}$, and the mass flow rate is the same as in Eq.(2). The local thrusting pitch and yaw steering angles have the same definitions as in Eq.(3) but referenced in the MCI coordinate. The moon's gravitational parameter and moon's radius (μ_{m} and R_{m}) also define the non-dimensional units in the MCI coordinate as follows

$$\tilde{d}_{\mathrm{m}} = R_{\mathrm{m}},\ \tilde{v}_{\mathrm{m}} = \sqrt{\frac{\mu_{\mathrm{m}}}{R_{\mathrm{m}}}},\ \tilde{t}_{\mathrm{m}} = \frac{R_{\mathrm{m}}}{\tilde{v}_{\mathrm{m}}},\ \tilde{a}_{\mathrm{m}} = R_{\mathrm{m}}/\tilde{t}_{\mathrm{m}}^2 \quad (9)$$

The moon's J_2 perturbations have the same formulation as in Eq.(5) with the substitutions of $J_{2\mathrm{m}}$, μ_{m}, and R_{m} for $J_{2\mathrm{e}}$, μ_{e}, and R_{e}.

The gravitational accelerations of the sun and the Earth expressed in the MCI coordinate can be written as

$$\tilde{\boldsymbol{\alpha}}_{\mathrm{sun}_2} = -\mu_{\mathrm{sun}}\left(\frac{\boldsymbol{r}_{\mathrm{sun-sc}}}{\|\boldsymbol{r}_{\mathrm{sun-sc}}\|^3} + \frac{\boldsymbol{r}_{\mathrm{m-sun}}}{\|\boldsymbol{r}_{\mathrm{m-sun}}\|^3}\right) \quad (10)$$

$$\tilde{\boldsymbol{\alpha}}_{\mathrm{Earth}} = -\mu_{\mathrm{m}}\left(\frac{\boldsymbol{r}_{\mathrm{e-sc}}}{\|\boldsymbol{r}_{\mathrm{e-sc}}\|^3} + \frac{\boldsymbol{r}_{\mathrm{m-e}}}{\|\boldsymbol{r}_{\mathrm{m-e}}\|^3}\right) \quad (11)$$

where $\boldsymbol{r}_{\mathrm{m-sun}}$ is the position vector from the moon to the sun, $\boldsymbol{r}_{\mathrm{e-sc}}$ from the Earth to the spacecraft, and $\boldsymbol{r}_{\mathrm{m-e}}$ from the moon to the Earth. Also, $\tilde{\boldsymbol{\alpha}}_{\mathrm{sun}_2}$ and $\tilde{\boldsymbol{\alpha}}_{\mathrm{Earth}}$ in the MCI coordinate should be transformed to $\boldsymbol{\alpha}_{\mathrm{sun}_2}$ and $\boldsymbol{\alpha}_{\mathrm{Earth}}$ in the local rotating coordinate.

3 Five Segments of the Earth-moon Trajectory

The entire Earth-moon trajectory is divided into five segments:

(1) Burn arc from LEO to HEO;

(2) Burn arc from HEO to the start of the trans-lunar coast arc;

(3) Trans-lunar coast arc;

(4) Burn arc from the end of trans-lunar coast arc to HLO;

(5) Burn arc from HLO to LLO.

Fig. 2 illustrates trajectory segments, and Table 1 summarizes perturbations, trajectory propagation methods, and inertial coordinates in different trajectory segments.

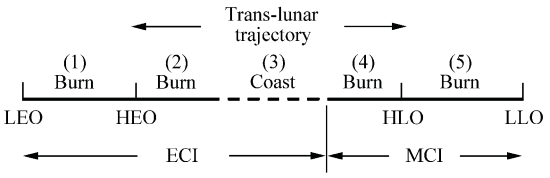

Fig. 2 Illustration of five trajectory segments.

Table 1 Different trajectory segments

Segment	Perturbations	Propagation method	Coordinate
(1)	Earth shadow, Earth J_2	AOAT	ECI
(2) , (3)	Earth J_2, moon gravity, sun gravity	Numerical integration	ECI
(4)	Moon J_2, Earth gravity, sun gravity	Numerical integration	MCI
(5)	Moon shadow, moon J_2	AOAT	MCI

It is well known that the low-thrust spirals from LEO to HEO and those from HLO to LLO consist of hundreds or even thousands of orbital revolutions, which requires a formidable amount of time to compute if trajectories are numerically integrated. Segments (2)-(4) having relatively fewer orbital revolutions are easier to be numerically integrated for moderate duration. Thus, the AOAT, a fast trajectory propagation algorithm, is used to compute the segments (1) and (5). For the segments (1)-(3), the trajectories in the ECI coordinate are propagated forward in time while those in segments (4) and (5) in the MCI coordinate backward in time. Since the gravitational forces of the sun, the Earth, and the moon in both ECI and MCI coordinates are considered, the optimization subroutine would automatically find the proper location to switch from the ECI coordinate to the MCI coordinate. Thus, it is not necessary to specify a fixed intermediate point requisite for the conventional patched conic method.

4 Computing Earth-orbit Ascending and Lunar Descending Trajectories Using AOAT

The tangential steering along the velocity direction is employed for the Earth-orbit ascending trajectory from LEO to HEO, while the anti-tangential steering for the lunar descending trajectory from HLO to LLO. Either the tangential or anti-tangential steering is the optimal control strategy to change the instantaneous rate of semi-major axis. The trajectory segments (1) and (5) computed by the AOAT are accurate only for relatively low orbits about an attracting body, where the J_2 perturbations and significant shadowing effect are included, but the insignificant third-body perturbations are ignored. The AOAT algorithm is described in Ref.[15] and also briefly presented in Appendix B. The primary advantage of the AOAT lies in the multi-revolution trajectories which can be quickly propagated while maintaining satisfactory accuracy[15]. Note that the computational procedure of the moon-capture trajectory using anti-tangential thrust is opposite to that using tangential-thrust trajectory.

Let the initial condition of classical orbit elements, mass, and time at LEO be

$$a_{\mathrm{t0}}^{(1)},\ e_{\mathrm{t0}}^{(1)},\ i_{\mathrm{t0}}^{(1)},\ \Omega_{\mathrm{t0}}^{(1)},\ \omega_{\mathrm{t0}}^{(1)},\ m_{\mathrm{t0}}^{(1)},\ t_{\mathrm{t0}}^{(1)}$$

where the superscripts represent the segment index number and the subscript "t0" denotes the initial time of the corresponding trajectory segment. The AOAT propagates the tangential-thrust trajectory and determines the orbital elements, spacecraft mass, and flight time at a point where the semi-major axis is pre-defined by $a_{\mathrm{tf}}^{(1)}$ with the subscript "tf" denoting the terminal time of the corresponding trajectory segment

$$a_{\mathrm{tf}}^{(1)},\ e_{\mathrm{tf}}^{(1)},\ i_{\mathrm{tf}}^{(1)},\ \Omega_{\mathrm{tf}}^{(1)},\ \omega_{\mathrm{tf}}^{(1)},\ m_{\mathrm{tf}}^{(1)},\ t_{\mathrm{tf}}^{(1)}$$

Likewise, for the segment (5) that is propagated backward in time, if the terminal condition at LLO is

$$a_{\mathrm{tf}}^{(5)},\ e_{\mathrm{tf}}^{(5)},\ i_{\mathrm{tf}}^{(5)},\ \Omega_{\mathrm{tf}}^{(5)},\ \omega_{\mathrm{tf}}^{(5)},\ m_{\mathrm{tf}}^{(5)},\ t_{\mathrm{tf}}^{(5)}$$

The initial condition of the segment (5) can be obtained by backward integrating anti-tangential-thrust trajectory to a point where the semi-major axis is pre-defined by $a_{\mathrm{t0}}^{(5)}$

$$a_{\mathrm{t0}}^{(5)},\ e_{\mathrm{t0}}^{(5)},\ i_{\mathrm{t0}}^{(5)},\ \Omega_{\mathrm{t0}}^{(5)},\ \omega_{\mathrm{t0}}^{(5)},\ m_{\mathrm{t0}}^{(5)},\ t_{\mathrm{t0}}^{(5)}$$

Note that the AOAT does not consider true anomaly, which is a variable to be optimized.

5 Optimization Method for Trans-lunar Trajectory Segments

A direct/indirect method is used to obtain near optimal control steering for trans-lunar trajectory from HLO to HLO. Note that this method is employed to solve an Earth-orbit transfer (Zondervan, Wood, and Caughey[16]), low-thrust Earth-moon transfers in the classical restricted three-body dynamics (Kluever and Pierson[5-8]) as well as interplanetary transfers (Gao and Kluever[17]). In this paper, the direct/indirect method is used in terms of the equinoctial elements. According to the calculus of variation theory, the Hamiltonian of optimal control problem takes the following form

$$H=\boldsymbol{\lambda}^{\mathrm{T}}\boldsymbol{M}\left(\frac{T}{m}\boldsymbol{\alpha}_{\mathrm{T}}+\boldsymbol{f}_{\mathrm{p}}\right)+\boldsymbol{\lambda}^{\mathrm{T}}\boldsymbol{D}-\lambda_{\mathrm{m}}\frac{T}{g_0 I_{\mathrm{sp}}} \tag{12}$$

where $\boldsymbol{f}_{\mathrm{p}}$ includes J_2 perturbations and third-body perturbations (in both ECI and MCI coordinates). $\boldsymbol{\lambda}=[\lambda_{\mathrm{p}}\ \ \lambda_{\mathrm{f}}\ \lambda_{\mathrm{g}}\ \lambda_{\mathrm{h}}\ \lambda_{\mathrm{k}}\ \lambda_{\mathrm{L}}]^{\mathrm{T}}$ is the costate vector associated with the corresponding equinoctial elements, and λ_{m} the costate variable associated with the spacecraft mass. The optimal control steering direction unit vector is obtained by setting $\partial H/\partial\boldsymbol{\alpha}_{\mathrm{T}}=0$ with the constraint $\|\boldsymbol{\alpha}_{\mathrm{T}}\|=1$.

$$\boldsymbol{\alpha}_{\mathrm{T}}^{*}=-\frac{[\boldsymbol{\lambda}^{\mathrm{T}}\boldsymbol{M}]^{\mathrm{T}}}{\left\|\boldsymbol{\lambda}^{\mathrm{T}}\boldsymbol{M}\right\|} \tag{13}$$

Taking the partial derivative of the Hamiltonian with respect to the states, the costate equations are determined.

$$\dot{\boldsymbol{\lambda}}=-\frac{\partial H}{\partial\boldsymbol{x}}=-\left(\boldsymbol{\lambda}^{\mathrm{T}}\frac{\partial\boldsymbol{M}}{\partial\boldsymbol{x}}\frac{T}{m}\boldsymbol{\alpha}_{\mathrm{T}}^{*}+\boldsymbol{\lambda}^{\mathrm{T}}\frac{\partial\boldsymbol{D}}{\partial\boldsymbol{x}}\right)-\left(\boldsymbol{\lambda}^{\mathrm{T}}\frac{\partial\boldsymbol{M}}{\partial\boldsymbol{x}}\boldsymbol{f}_{\mathrm{p}}+\boldsymbol{\lambda}^{\mathrm{T}}\boldsymbol{M}\frac{\partial\boldsymbol{f}_{\mathrm{p}}}{\partial\boldsymbol{x}}\right) \tag{14}$$

$$\dot{\lambda}_{\mathrm{m}}=-\frac{\partial H}{\partial m}=\boldsymbol{\lambda}^{\mathrm{T}}\boldsymbol{M}\frac{T}{m^2}\boldsymbol{\alpha}_{\mathrm{T}}^{*}=-\left\|\boldsymbol{\lambda}^{\mathrm{T}}\boldsymbol{M}\right\|\frac{T}{m^2} \tag{15}$$

It indicates that the optimal control is governed by costate variables whose dynamics are given by

Eq.(19). For simplicity, the costate dynamics associated with the two-body dynamic model is used to govern the control steering to make deriving derivatives of $\boldsymbol{f}_{\mathrm{p}}$ with respect to the states unnecessary. In fact, the third-body perturbations are time-varying function without explicit derivatives with respect to equinoctial elements. However, the equations of motion do include perturbations. The initial costate variables or terminal costate variables need to be guessed to satisfy the necessary boundary constraints without regard to the transversality condition and time-varying condition, which should be considered in a classical two-point boundary-value problem. The optimal objective function and boundary conditions are all treated by nonlinear optimization programming. Since the costate variable associated with mass do not affect the optimal control, the first six costate variables (λ_{m} is not used) could be used. Thus, for the segment (2), the state equations are Eq.(1) and Eq.(16) and the costate equation is Eq.(17).

$$\dot{m}=-\frac{T}{g_0 I_{\mathrm{sp}}} \quad \text{where} \quad T=\frac{2\eta P}{g_0 I_{\mathrm{sp}}} \tag{16}$$

$$\dot{\boldsymbol{\lambda}}=-\frac{\partial H}{\partial \boldsymbol{x}}=-\left(\boldsymbol{\lambda}^{\mathrm{T}}\frac{\partial \boldsymbol{M}}{\partial \boldsymbol{x}}\boldsymbol{\alpha}_{\mathrm{T}}^{*}+\boldsymbol{\lambda}^{\mathrm{T}}\frac{\partial \boldsymbol{D}}{\partial \boldsymbol{x}}\right) \tag{17}$$

Likewise, for the segment (4), the state equations are Eq.(9) and Eq.(16), and the costate equation has the same form as in Eq.(17), but referenced in the MCI. The advantage of the direct/indirect method over the direct transcription method lies in fewer variables and constraints leading to saving on considerable time for computation. However, the costate variables needed to be integrated have no intuitive physical meaning, which makes optimization problem much harder to converge although some techniques such as the adjoint-control transformation[18] and the multiple-shooting technique[17] are helpful in improving convergence robustness.

The initial condition of the segment (2) can be denoted by state variables $\boldsymbol{x}_{\mathrm{t0}}^{(2)}$ and costate variables $\boldsymbol{\lambda}_{\mathrm{t0}}^{(2)}$, where $\boldsymbol{x}_{\mathrm{t0}}^{(2)}$ expressed in equinoctial elements $[p_{\mathrm{t0}}^{(2)}\ f_{\mathrm{t0}}^{(2)}\ g_{\mathrm{t0}}^{(2)}\ h_{\mathrm{t0}}^{(2)}\ k_{\mathrm{t0}}^{(2)}]$ is transformed from $a_{\mathrm{tf}}^{(1)}, e_{\mathrm{tf}}^{(1)}, i_{\mathrm{tf}}^{(1)}, \Omega_{\mathrm{tf}}^{(1)}, \omega_{\mathrm{tf}}^{(1)}$, and $m_{\mathrm{t0}}^{(2)}=m_{\mathrm{tf}}^{(1)}$, $t_{\mathrm{t0}}^{(2)}=t_{\mathrm{tf}}^{(1)}$. The initial values of true longitude $L_{\mathrm{t0}}^{(2)}$ and costate variables need to be guessed. The segment (3) does not integrate the costate equations since there is no thrust during the coast arc. The initial condition of the segment (3) is the terminal condition of the segment (2). In contrast, the segment (4) is integrated backward, and the terminal condition of the segment (4) is state variables $\boldsymbol{x}_{\mathrm{tf}}^{(4)}$ and costate variables $\boldsymbol{\lambda}_{\mathrm{tf}}^{(4)}$, where $\boldsymbol{x}_{\mathrm{tf}}^{(4)}$ in equinoctial elements $[p_{\mathrm{tf}}^{(4)}\ f_{\mathrm{tf}}^{(4)}\ g_{\mathrm{tf}}^{(4)}\ h_{\mathrm{tf}}^{(4)}\ k_{\mathrm{tf}}^{(4)}]$ are transformed from $a_{\mathrm{t0}}^{(5)}, e_{\mathrm{t0}}^{(5)}, i_{\mathrm{t0}}^{(5)}, \Omega_{\mathrm{t0}}^{(5)}, \omega_{\mathrm{t0}}^{(5)}$ and $m_{\mathrm{tf}}^{(4)}=m_{\mathrm{t0}}^{(5)}$, $t_{\mathrm{tf}}^{(4)}=t_{\mathrm{t0}}^{(5)}$. The terminal values of true longitude $L_{\mathrm{tf}}^{(4)}$ and costate variables need to be guessed. Obviously, a complete trajectory should satisfy the following constraint

$$[p_{\mathrm{tf}}^{(3)}\ f_{\mathrm{tf}}^{(3)}\ g_{\mathrm{tf}}^{(3)}\ h_{\mathrm{tf}}^{(3)}\ k_{\mathrm{tf}}^{(3)}\ L_{\mathrm{tf}}^{(3)}\ m_{\mathrm{tf}}^{(3)}\ t_{\mathrm{tf}}^{(3)}]=$$
$$[p_{\mathrm{t0}}^{(4)}\ f_{\mathrm{t0}}^{(4)}\ g_{\mathrm{t0}}^{(4)}\ h_{\mathrm{t0}}^{(4)}\ k_{\mathrm{t0}}^{(4)}\ L_{\mathrm{t0}}^{(4)}\ m_{\mathrm{t0}}^{(4)}\ t_{\mathrm{t0}}^{(4)}]$$

6 Formulation of Nonlinear Optimization Problem

In the Section 4 and Section 5, the AOAT and the direct/indirect method are described, and the initial/ terminal conditions are specified for each burn segment. The next step is to formulate a parameter optimization problem that is in turn solved by nonlinear programming—sequential quadratic programming (SQP), in which the overall mission objective is to minimize the propellant consumption during the transfer. The SQP variables and constraints are summarized as follows

22 SQP variables:

11 variables in the forward trajectory propagation for segments (1)-(3):

Segment (1): LEO departure date $t_{\mathrm{t0}}^{(1)}$, LEO's $\Omega_{\mathrm{t0}}^{(1)}$;

Segment (2): six initial costate variables $\boldsymbol{\lambda}_{\mathrm{t0}}^{(2)}$ for the Earth-departure burn arc, burn arc duration $t_{\mathrm{tf}}^{(2)}$-$t_{\mathrm{t0}}^{(2)}$, HEO's longitude angle $L_{\mathrm{t0}}^{(2)}$;

Segment (3): coast arc duration $t_{\mathrm{tf}}^{(3)}$-$t_{\mathrm{t0}}^{(3)}$.

11 variables in the backward trajectory propagation for segments (4) and (5):

Segment (4): six terminal costate variables $\boldsymbol{\lambda}_{\mathrm{tf}}^{(4)}$ for the moon-capture burn arc, burn arc duration $t_{\mathrm{tf}}^{(4)}$-$t_{\mathrm{t0}}^{(4)}$, HLO's longitude angle $L_{\mathrm{tf}}^{(4)}$;

Segment (5): LLO departure date $t_{tf}^{(5)}$, spacecraft mass at LLO $m_{tf}^{(5)}$, LLO's $\Omega_{tf}^{(5)}$.

8 SQP equality constraints:

6 constraints: terminal states of segment (3) = initial states of segment (4);

1 constraint: date at the terminal time of segment (3) = date at the initial time of segment (4);

1 constraint: mass at the terminal time of segment (3) = mass at the initial time of segment (4) .

7 Comparison with Direct Transcription Method

The direct transcription method parameterizes the control history using discrete nodes, which inevitably results in a large number of variables and constraints if the transfer contains much more revolutions. In this paper, with the help of costate equations, the formulated SQP problem involves only 22 variables and 8 constraints, which is generally regarded as a smaller dimensional nonlinear optimization. Another focused point is the use of the AOAT, a semi-analytic method for trajectory propagation. Capable of propagating hundreds or even thousands of revolutions, it is much faster than precise numerical integration.

Compared with the direct transcription method, the proposed method reduces computational time by orders, especially for long-duration multi-revolution transfers. This makes it possible to optimize the entire transfer trajectory as a single nonlinear optimization problem.

8 Numerical Results

An Earth-moon trajectory from a LEO with 500 km altitude to a LLO with 200 km altitude is presented. First, the parameters of the spacecraft to be defined are: the input power of the solar electric propulsion $P = 10$ kW, the efficiency $\eta = 0.65$, the specific impulse $I_{sp} = 3\,300$ s, and the initial spacecraft mass set to be 1 000 kg. Thus, the calculated initial thrust-to-weight ratio (T/m_0g_0) equals to $4.096\,3\times10^{-5}$. The parameters of the initial LEO and the terminal LLO are specified in Table 2. The initial Earth departure date is set to be Jan. 1, 2008. Note that the 90° inclination of the LLO is referenced in the MCI coordinate defined in this paper. In fact, 90° might not be an ideal inclination of a LLO parking orbit for the spacecraft, which should take into account the moon's obliquity angle, angle between the moon's rotation axis and the Earth equatorial plane or ecliptic plane, and further detailed analysis of lunar gravity field. Falling out of the scope of this paper, this problem will not be discussed.

Table 2 Initial LEO and terminal LLO

Orbital elements	Initial LEO	Terminal LLO
Semi-major axis	$1.078\,4\ R_e$	$1.115\,1\ R_m$
Eccentricity	0.001	0.001
Inclination/(°)	28.5	90.0
Ascension of ascending node	free	free
Argument of periapsis/(°)	0	0
True anomaly	free	free

As described in previous sections, the AOAT computes trajectory segment from the LEO to a HEO ($a_{HEO} = 10R_e$) in the ECI coordinate. It goes the same way for the AOAT to compute the trajectory segment from the LLO to a HLO ($a_{HLO} = 2R_m$) in the MCI. As shown in Ref.[15], the lower the altitudes of HEO and HLO, the more accurate the solutions. However, the low attitudes might result in more revolutions for the trans-lunar trajectory segment, which will conceptually cause difficulties in converging if the indirect/direct method is used. But, if the number of revolution is not excessively large for instance under 50, the indirect/direct method still works well without too many troubles guessing initial costate variables. The indirect/direct method was once used to solve a lot of transfer problems with small numbers of revolutions[6-8]. On the base of previous researches and author's experience in trajectory optimization, $a_{HEO} = 10R_e$ and $a_{HLO} = 2R_m$ are selected in the following example.

The formulated parameter optimization problem has a small number of variables and constraints. However, it appears not easy to make initial guesses for 22 SQP variables to obtain converged solutions at the first run. As a result, the following steps are

taken to find out the final optimal solutions:

Step 1 To generate a trajectory to rendezvous moon in the ECI coordinate with a burn-coast-burn engine sequence exclusive of the lunar perturbation. In this step, the lunar capture is not considered.

Step 2 To remove the second burn and adjust the duration of the first burn and coast arcs to make the end of the coast arc in the vicinity of moon.

Step 3 To generate a trajectory in the MCI coordinate to escape moon's gravity and try different values for SQP variables in the segments (4) and (5) to make 8 SQP equality constraints as close as possible.

Step 4 To optimize the trajectories from the LEO to the LLO in a single SQP problem based on the solutions obtained from Step 3.

After performing the Step 4, the obtained LEO-LLO trajectories are summarized in Table 3, which shows about 80 days left for the trans-lunar trajectory from the HEO to the HLO. The Earth-orbit ascending trajectory takes about 161 days and the moon descending trajectory about 12 days. Through AOAT, are obtained about 1 009 orbital revolutions from the LEO to the HEO, and about 94 revolutions from the HLO to the LLO. It indicates that the trajectories computed by the AOAT have majority of revolutions of the entire transfer trajectory, and take about almost half the transfer time.

Table 3 Solutions for the LEO-LLO trajectories

Mission parameters	Solutions
LEO departure date	Dec. 31, 2007
HEO arrival date	June 10,2008
Duration from LEO to HEO/day	161.58
1^{st} burn arc duration (trans-lunar)/day	50.32
coast arc duration (trans-lunar)/day	9.49
2^{nd} burn arc duration (trans-lunar)/day	19.42
HLO arrival date	Aug. 28, 2008
LLO arrival date	Sept. 9, 2008
Duration from HLO to LLO/day	12.37
Total transfer time/day	253.18
Final mass at LLO/kg	791.31

The time histories of semi-major axis, eccentricity, and inclination in both ECI and MCI coordinates are presented in Figs.3-5, respectively, from which it is clear that semi-major axis increases in the ECI coordinate and decreases in the MCI coordinate. From the LEO to the HEO, the eccentricity is raised at first to about 0.16 followed by slightly falling and then quickly increasing. In the moon-capture phase, the eccentricity is about 0.14 at the HLO. The eccentricity does not change monotonically mainly because of the effect of shadow. Without the shadowing effect, the trajectory from the LEO to the HEO or from HLO to the LLO should be a near-circular transfer. The inclination change in the MCI coordinate is not significant since the spacecraft enters moon-capture trajectory with an optimally chosen orientation. Additionally, the transfer trajectories in the ECI coordinate are presented in Fig.6, and the lunar capture trajectory in Fig.7. The control steering direction angles in both ECI and MCI coordinates are presented in Fig.8 and Fig.9.

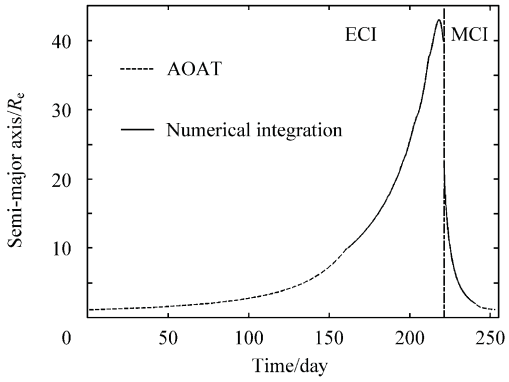

Fig.3 Time history of semi-major axis from LEO to LLO.

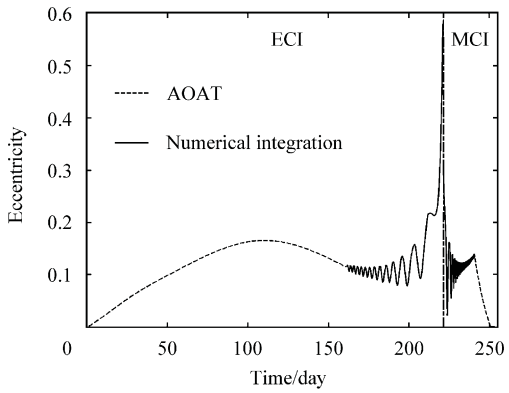

Fig.4 Time history of eccentricity from LEO to LLO.

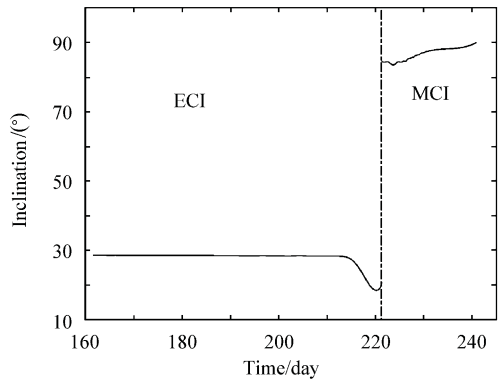

Fig.5 Time history of inclination from HEO to HLO.

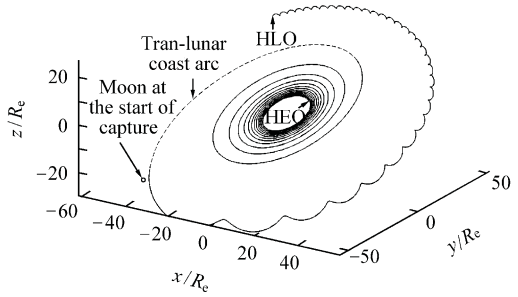

Fig.6 Trajectory from HEO to HLO in the ECI coordinate.

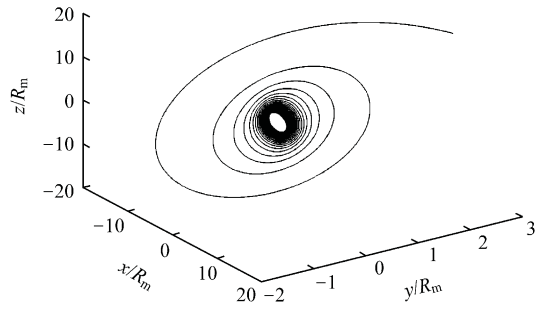

Fig.7 Moon-capture trajectory to HLO in the MCI coordinate.

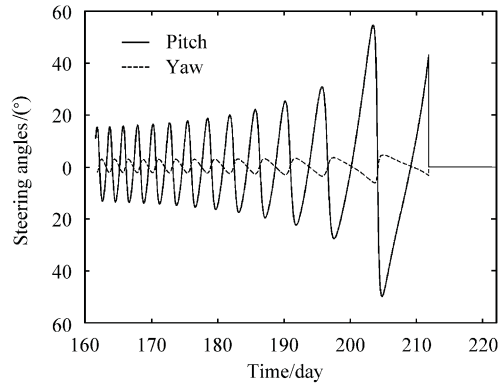

Fig.8 Time histories of control steering for trajectory from HEO to escape (ECI).

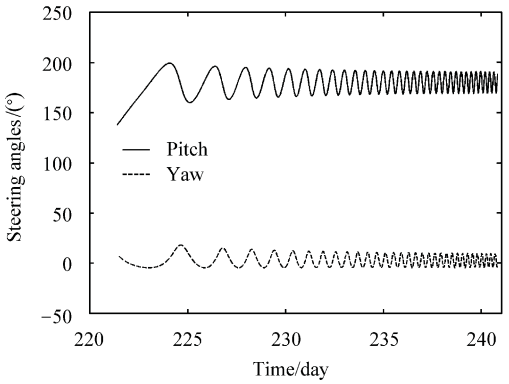

Fig.9 Time histories of control steering for trajectory from capture to HEO (MCI).

9 Conclusions

A feasible method has been proposed to find preliminary solutions for Earth-moon transfer trajectories from LEO to LLO using SEP. The shadow effects, oblateness of the Earth and the moon, the gravitational forces of the sun, the Earth, and the moon are all taken into consideration, and the trajectories are solved using a practical, complex three-dimensional dynamic model. The JPL planetary and lunar ephemerides are utilized to compute precise positions of involved celestial bodies. The significant shadowing effect at relatively low altitude orbits is considered to highlight the use of solar electric propulsion. By means of AOAT and the direct/indirect method, the optimal orbit transfer problem can be converted to a parameter optimization problem that only involves a small number of SQP variables and constraints. The main advantage of the proposed method lies in its provision of a more efficient algorithm to optimize long-duration, multi-revolution transfer trajectories while keeping the solution satisfactorily accurate. The obtained solutions can be used as a good initial guess for further trajectory optimization problems in high-fidelity dynamic models.

References

[1] Rayman M D, Williams S N. Design of the first interplanetary solar electric propulsion mission. Journal of Spacecraft and Rockets 2002; 39(4): 589-595.

[2] Koppel C R, Marchandise F, Estublier D, et al. The SMART-1

electric propulsion subsystem in flight experience. AIAA Paper-2004-3435, 2004.

[3] Golan O M, Breakwell J V. Minimum fuel lunar trajectories for a low-thrust power-limited spacecraft. AIAA Paper 90-2975, 1990.

[4] Guelman M. Earth-to-moon transfer with a limited power engine. Journal of Guidance, Control, and Dynamics 1995; 18(5): 1133-1138.

[5] Pierson B L, Kluever C A. Three-stage approach to optimal low-thrust earth-moon trajectories. Journal of the Astronautical Sciences 1994; 42(3): 269-283.

[6] Kluever C A, Pierson B L. Vehicle-and-trajectory optimization of nuclear electric spacecraft for lunar missions. Journal of Spacecraft and Rockets 1995; 32(1): 126-132.

[7] Kluever C A, Pierson B L. Optimal low-thrust three-dimensional earth-moon trajectories. Journal of Guidance, Control, and Dynamics 1995; 18(4): 830-837.

[8] Kluever C A, Pierson B L. Optimal earth-moon trajectories using nuclear electric propulsion. Journal of Guidance, Control, and Dynamics 1997; 20(2): 239-245.

[9] Herman A L, Bruce B A. Optimal, low-thrust, earth-moon orbit transfer. Journal of Guidance, Control, and Dynamics 1998; 21(1): 141-147.

[10] Betts J T, Erb S O. Optimal low thrust trajectory to the moon. SIAM Journal of Applied Dynamical System 2003; 2(2): 144-170.

[11] Standish E M. The JPL planetary and lunar ephemerides DE402/LE402. Bulletin of the American Astronomical Society 1995; 27: 1203.

[12] Walker M J H, Ireland B, Owens J. A set of modified equinoctial orbit elements. Celestial Mechanics 1985; 36(4): 409-419.

[13] Betts J T. Optimal interplanetary orbit transfers by direct transcription. Journal of the Astronautical Sciences 1994; 42(3): 247-268.

[14] Kluever C A. Optimal low-thrust interplanetary trajectories by direct method techniques. Journal of the Astronautical Sciences 1997; 45(3): 247-262.

[15] Gao Y, Kluever C A. Analytic orbital averaging technique for computing tangential-thrust trajectories. Journal of Guidance, Control and Dynamics 2005; 28(6): 1320-1323.

[16] Zondervan K P, Wood L J, Caughey T K. Optimal low-thrust, three-burn orbit transfers with large plane changes. Journal of the Astronautical Sciences 1984; 32(3): 407-427.

[17] Gao Y, Kluever C A. Low-thrust interplanetary orbit transfers using hybrid trajectory optimization method with multiple shooting. AIAA Paper-2004-5088, 2004.

[18] Dixon L C, Bartholomew-Biggs M C. Adjoint control transformations for solving practical optimal control problems. Optimal Control Applications and Methods 1981; 2(4): 365-381.

[19] Battin R H. An introduction to the mathematics and methods of astrodynamics. AIAA Education Serials. Washington, DC: AIAA, 1987: 488-489.

[20] Neta B, Vallado D. On satellite umbra/penumbra entry and exit positions. Journal of the Astronautical Sciences 1998; 46(1): 91-104

Biography:

Gao Yang Born in 1974, he received B.S. degree from Beijing University of Aeronautics and Astronautics in 1997 and M.S. degree from Chinese Academy of Sciences in 2000. He received his doctoral degree in 2003 from the University of Missouri-Columbia, USA. From 2004 to 2005, he was a postdoctoral research fellow in the University of Missouri-Columbia. Since June 2005, he has been an associate research fellow at Academy of Opto-Electronic, Chinese Academy of Sciences. His research interests include orbital mechanics, spacecraft dynamics and control, guidance and navigation, trajectory optimization, and space mission design.

E-mail: gaoy@aoe.ac.cn

Appendix A: Matrices *M* and *D*

The elements of matrices ***M***, ***D*** expressed by equinoctial elements are as follows

$$\boldsymbol{M}=\begin{bmatrix} M_{11} & M_{12} & M_{13} \\ M_{21} & M_{22} & M_{23} \\ M_{31} & M_{32} & M_{33} \\ M_{41} & M_{42} & M_{43} \\ M_{51} & M_{52} & M_{53} \\ M_{61} & M_{62} & M_{63} \end{bmatrix}$$

$$M_{11}=0\ ,\ M_{12}=\frac{2p}{w}\sqrt{\frac{p}{\mu}}\ ,\ M_{13}=0\ ,\quad M_{21}=\sqrt{\frac{p}{\mu}}\sin L$$

$$M_{22}=\sqrt{\frac{p}{\mu}}[(w+1)\cos L+f]\frac{1}{w}$$

$$M_{23}=-\sqrt{\frac{p}{\mu}}(h\sin L-k\cos L)\frac{g}{w}$$

$$M_{31}=-\sqrt{\frac{p}{\mu}}\cos L,\quad M_{32}=\sqrt{\frac{p}{\mu}}[(w+1)\sin L+g]\frac{1}{w}$$

$$M_{33}=\sqrt{\frac{p}{\mu}}(h\sin L-k\cos L)\frac{f}{w}$$

$$M_{41}=M_{42}=0,\quad M_{43}=\sqrt{\frac{p}{\mu}}\frac{s^2}{2w}\cos L$$

$$M_{51}=M_{52}=0,\quad M_{53}=\sqrt{\frac{p}{\mu}}\frac{s^2}{2w}\sin L$$

$$M_{61}=M_{62}=0,\quad M_{63}=\frac{1}{w}\sqrt{\frac{p}{\mu}}(h\sin L-k\cos L)$$

$$\boldsymbol{D}=[0\ 0\ 0\ 0\ 0\ D_6]^{\mathrm{T}},\quad D_6=\sqrt{\mu p}\left(\frac{w}{p}\right)^2$$

where $w=1+f\cos L+g\sin L$, μ is the Earth gravitational parameter, and $s^2=1+h^2+k^2$. The equinoctial elements can be obtained in terms of classical orbital elements (a, e, i, Ω, ω, θ):

$p=a(1-e^2)$, $f=e\cos(\omega+\Omega)$, $g=e\sin(\omega+\Omega)$,

$h=\tan(i/2)\cos\Omega$, $k=\tan(i/2)\sin\Omega$,

$L=\Omega+\omega+\theta$ where θ is true anomaly.

Appendix B: Analytic Orbital Averaging Technique

In this section, equations are deduced in the ECI coordinate, which in the MCI coordinate can be deduced likewise. In order to obtain the analytic incremental changes using tangential-thrust in classical orbital elements, it is preferable to start with the Gauss planetary equations[17]:

$$\frac{\mathrm{d}a}{\mathrm{d}t}=\frac{2a^2e\sin\theta}{h^*}f_r+\frac{2a^2p}{h^*r}f_\theta \tag{B1}$$

$$\frac{\mathrm{d}e}{\mathrm{d}t}=\frac{1}{h^*}p\sin\theta\ f_r+\frac{1}{h^*}[(p+r)\cos\theta+re]f_\theta \tag{B2}$$

$$\frac{\mathrm{d}\omega}{\mathrm{d}t}=-\frac{p\cos\theta}{h^*e}f_r+\frac{(p+r)\sin\theta}{h^*e}f_\theta \tag{B3}$$

$$\frac{\mathrm{d}E}{\mathrm{d}t}=\frac{na}{r}+\frac{1}{nae}[f_r(\cos\theta-e)-f_\theta(1+\frac{r}{a})\sin\theta] \tag{B4}$$

where $p=a(1-e^2)$, $h^*=\sqrt{\mu p}$, $n=\sqrt{\mu/a^3}$, and $r=p/(1+e\cos\theta)$. When the thrust acceleration (f_r and f_θ) is much smaller than the gravitational acceleration, the derivative of eccentric anomaly with respect to time is approximated by removing the thrust term

$$\frac{\mathrm{d}E}{\mathrm{d}t}\approx\frac{na}{r} \tag{B5}$$

After transforming eccentric anomaly E to true anomaly θ by

$$\sin\theta=\frac{\sin E\sqrt{1-e^2}}{1-e\cos E}\ ,\quad \cos\theta=\frac{\cos E-e}{1-e\cos E} \tag{B6}$$

the derivatives of the first five classical orbital elements (a, e, i, Ω, ω, θ) with respect to eccentric anomaly can be computed by dividing the Gauss planetary equations (B1)-(B4) by Eq.(B5):

$$\frac{\mathrm{d}a}{\mathrm{d}E}=\frac{2a^3}{\mu}\left(f_re\sin E+f_\theta\sqrt{1-e^2}\ \right) \tag{B7}$$

$$\frac{\mathrm{d}e}{\mathrm{d}E}=\frac{a^2}{\mu}\Big(f_r(1-e^2)\sin E+f_\theta(2\cos E-e-e\cos^2E)\sqrt{1-e^2}\Big) \tag{B8}$$

$$\frac{\mathrm{d}\omega}{\mathrm{d}E}=-\cos i\frac{\mathrm{d}\Omega}{\mathrm{d}E}-\frac{a^2}{e\mu}\Big(f_r(\cos E-e)\sqrt{1-e^2}-f_\theta(2-e^2-e\cos E)\sin E\Big) \tag{B9}$$

The thrust is so low that it can be assumed that over an orbital arc the classical orbital elements and acceleration are kept constant. The steering that maximizes the rate of semi-major axis (i.e., tangential steering) can be derived by setting $\partial(\mathrm{d}a/\mathrm{d}E)/\partial\alpha=0$ and $\partial^2(\mathrm{d}a/\mathrm{d}E)/\partial\alpha^2<0$

$$\sin\alpha=\frac{e\sin E}{\sqrt{1-e^2\cos^2E}},\cos\alpha=\frac{\sqrt{1-e^2}}{\sqrt{1-e^2\cos^2E}} \tag{B10}$$

The analytic expressions for integrals with respect to eccentric anomaly are:

$$\int_{E_0}^{E_\mathrm{f}}\frac{\mathrm{d}a}{\mathrm{d}E}\mathrm{d}E=\frac{2a^3}{\mu}f_{\mathrm{in}}\int_{E_0}^{E_\mathrm{f}}\sqrt{1-e^2\cos^2E}\mathrm{d}E \tag{B11}$$

$$\int_{E_0}^{E_\mathrm{f}}\frac{\mathrm{d}e}{\mathrm{d}E}\mathrm{d}E=\frac{2a^2}{e\mu}(1-e^2)f_{\mathrm{in}}\left\{\int_{E_0}^{E_\mathrm{f}}\sqrt{1-e^2\cos^2E}\mathrm{d}E-\int_{E_0}^{E_\mathrm{f}}1\Big/\sqrt{1-e^2\cos^2E}\ \mathrm{d}E+[\ln(\sin E+\sqrt{1-e^2\cos^2E}\,/e)]_{E_0}^{E_\mathrm{f}}\right\} \tag{B12}$$

$$\int_{E_0}^{E_\mathrm{f}}\frac{\mathrm{d}\omega}{\mathrm{d}E}\mathrm{d}E=-\frac{2a^2}{e^2\mu}\sqrt{1-e^2}f_{\mathrm{in}}\bullet\left[\sqrt{1-e^2\cos^2E}+\sin^{-1}(e\cos E)\right]_{E_0}^{E_\mathrm{f}} \tag{B13}$$

where f_{in} is acceleration amplitude. Note that it is unable to find analytic expressions for the terms $\int_{E_0}^{E_f}\sqrt{1-e^2\cos^2 E}\,\mathrm{d}E$ and $\int_{E_0}^{E_f}\frac{1}{\sqrt{1-e^2\cos^2 E}}\mathrm{d}E$. The following approximations can be utilized for these functions to be integrated.

$$\sqrt{1-e^2\cos^2 E}\approx\sqrt{1-e^2}+(1-\sqrt{1-e^2})\sin^2 E \quad \text{(B14)}$$

$$\sqrt{1-e^2\cos^2 E}-\frac{1}{\sqrt{1-e^2\cos^2 E}}=\frac{-e^2\cos^2 E}{\sqrt{1-e^2\cos^2 E}}\approx\frac{-e^2\cos^2 E}{\sqrt{1-e^2c}} \quad \text{(B15)}$$

To make the functions and their approximations as close as possible, $c = 0.8$ is chosen by way of trial-and-error tests. The corresponding integrals are then obtained in the following analytic forms:

$$\int_{E_0}^{E_f}\sqrt{1-e^2\cos^2 E}\,\mathrm{d}E\approx\left[\sqrt{1-e^2}E+(1-\sqrt{1-e^2})(0.5E-0.25\sin 2E)\right]_{E_0}^{E_f} \quad \text{(B16)}$$

$$\int_{E_0}^{E_f}\sqrt{1-e^2\cos^2 E}\,\mathrm{d}E-\int_{E_0}^{E_f}\frac{1}{\sqrt{1-e^2\cos^2 E}}\mathrm{d}E\approx\frac{-e^2}{\sqrt{1-e^2c}}\left[0.5E+0.25\sin 2E\right]_{E_0}^{E_f} \quad \text{(B17)}$$

Furthermore, the averaging changes of orbital elements due to J_2 perturbation are as follows:

$$\frac{\mathrm{d}\bar{a}}{\mathrm{d}t}=\frac{\mathrm{d}\bar{e}}{\mathrm{d}t}=\frac{\mathrm{d}\bar{i}}{\mathrm{d}t}=0 \quad \text{(B18)}$$

$$\frac{\mathrm{d}\bar{\Omega}}{\mathrm{d}t}=-\frac{3}{2}J_2\frac{R_e^{\ 2}}{a^2(1-e^2)^2}n\cos i \quad \text{(B19)}$$

$$\frac{\mathrm{d}\bar{\omega}}{\mathrm{d}t}=\frac{3}{4}J_2\frac{R_e^{\ 2}}{a^2(1-e^2)^2}n(5\cos^2 i-1) \quad \text{(B20)}$$

The increments in classical orbital elements and time including J_2 perturbations and cylindrical shadow[20] per revolution are approximated as:

$$\Delta\boldsymbol{z}=\int_{E_{ex}}^{E_{en}}\frac{\mathrm{d}\boldsymbol{z}}{\mathrm{d}E}\mathrm{d}E+\frac{\mathrm{d}\bar{\boldsymbol{z}}}{\mathrm{d}t}\frac{2\pi}{n} \quad \text{(B21)}$$

$$\Delta t=\frac{2\pi}{n} \quad \text{(B22)}$$

where $\boldsymbol{z}=[\,a,\ e,\ i,\ \Omega,\ \omega,\ \theta\,]$. The mass loss per revolution is computed by Earth shadow entrance and exit angles.

$$\Delta m=-\frac{2\eta P}{(g_0 I_{sp})^2}\left[\frac{1}{n}(E_{en}-e\sin E_{en}-E_{ex}+e\sin E_{ex})\right] \quad \text{(B23)}$$

With $\boldsymbol{y}=[\boldsymbol{z}\ \ t\ \ m]$ and $\Delta\boldsymbol{y}=[\Delta\boldsymbol{z}\ \ \Delta t\ \ \Delta m]$, the elements in the ($i$+1)th revolution is computed only in terms of the elements in the (i)th revolution

$$\boldsymbol{y}_{i+1}=\boldsymbol{y}_i+\Delta\boldsymbol{y}_i \quad \text{(B24)}$$

A terminal semi-major axis can be specified for the stop condition of the orbital averaging. The states at the terminal semi-major are obtained by interpolating the orbital elements during the last revolution

$$\boldsymbol{y}_{tf}=\boldsymbol{y}_i+\frac{a_{tf}-a_i}{a_{i+1}-a_i}(\boldsymbol{y}_{i+1}-\boldsymbol{y}_i) \quad \text{(B25)}$$